

Active Microrheology in Active Matter Systems: Mobility, Intermittency and Avalanches

C. Reichhardt and C. J. Olson Reichhardt

Theoretical Division, Los Alamos National Laboratory, Los Alamos, New Mexico 87545 USA

(Dated: February 23, 2015)

We examine the mobility and velocity fluctuations of a driven particle moving through an active matter bath of self-mobile disks for varied density or area coverage and varied activity. We show that the driven particle mobility can exhibit non-monotonic behavior that is correlated with distinct changes in the spatio-temporal structures that arise in the active media. We demonstrate that the probe particle velocity distributions exhibit specific features in the different dynamic regimes, and identify an activity-induced uniform crystallization that occurs for moderate activity levels and that is distinct from the previously observed higher activity cluster phase. The velocity distribution in the cluster phase has telegraph noise characteristics produced when the probe particle moves alternately through high mobility areas that are in the gas state and low mobility areas that are in the dense phase. For higher densities and large activities, the system enters what we characterize as an active jamming regime. Here the probe particle moves in intermittent jumps or avalanches which have power-law distributed sizes that are similar to the avalanche distributions observed for non-active disk systems near the jamming transition.

I. INTRODUCTION

In active microrheology, the properties of a medium are probed using the mobility and velocity fluctuations of an externally driven probe particle that is roughly the same size as the particles that comprise the medium¹⁻⁴. For example, the nonlinear mobility of a probe particle dragged through a colloidal system changes across the glass transition⁵⁻⁸. Other studies have examined anomalous diffusion properties of the probe^{9,10}, features of the driven particle velocity fluctuations, and threshold-to-motion or depinning type phenomena¹¹⁻¹³. In ordered systems, a driven particle can induce localized melting¹⁴ or shear thinning effects¹⁵. Driven particles or intruders have also been used to study the onset of jamming as a function of the system density¹⁶⁻²⁰. As the jamming transition is approached, the particle mobility is strongly reduced, its motion becomes increasingly intermittent, and just at jamming the velocity fluctuations become power-law distributed¹⁶⁻¹⁸.

Most active microrheology studies have focused on systems where the particles comprising the medium are not driven or experience only thermal fluctuations. There is, however, another class of systems to which the techniques of active microrheology can be applied: collections of self-motile particles or active matter^{21,22}. Examples of such systems include run-and-tumble bacteria²³⁻²⁶ or self-mobile colloidal particles²⁷⁻³³, which are commonly modeled as self-mobile sterically interacting particles undergoing either active Brownian motion or run-and-tumble dynamics. Such systems exhibit a transition from a uniform liquid state at low activities and densities to a cluster or phase separated state at higher activities and densities, where close-packed clusters are surrounded by a low density gas³²⁻⁴⁰. For monodisperse particles confined to two dimensions, the clusters have local triangular ordering, and the resulting crystallites can move, break apart, and re-form^{32,33,37-40}. A driven

probe particle in an active matter system should show clear changes in mobility or velocity fluctuations depending on the spatio-temporal behavior exhibited by the active matter, and thus could serve as a powerful tool for understanding a wide range of active systems. In numerical and theoretical studies of a driven probe particle in an active nematic system, anomalous viscosity effects such as a negative drag were predicted⁴¹. Experiments on cargo transport through crowded living cells showed that motion occurs in intermittent bursts which exhibit scaling behavior similar to that found in critical jammed solids⁴².

Here we examine the dynamics of a probe particle driven through a bath of run-and-tumble sterically interacting particles for varied activity or run length and varied particle density, the term we use for the area fraction covered by the disks. We show that the probe mobility and velocity fluctuations are correlated with distinct dynamic spatial structures that form in the bath. At low densities the probe mobility decreases with increasing run length, while the transition from a uniform active liquid to a phase separated cluster state coincides with a pronounced mobility drop. At high densities the mobility becomes an increasingly non-monotonic function of the activity. When the activity is low and the density is high, the system is disordered and the mobility is high. When the run length is increased slightly until it nearly matches the average spacing between the surfaces of neighboring particles, a uniform nearly crystalline state emerges that is correlated with a drop in the mobility by several orders of magnitude. As the run length is further increased, this crystalline state becomes disordered, the system enters a liquid phase, and the mobility increases by an order of magnitude or more. For large run lengths the system transitions from the liquid state to a phase-separated state, in which the mobility drops again. At high density and the largest run lengths, the system forms what we call an actively jammed state characterized by strongly

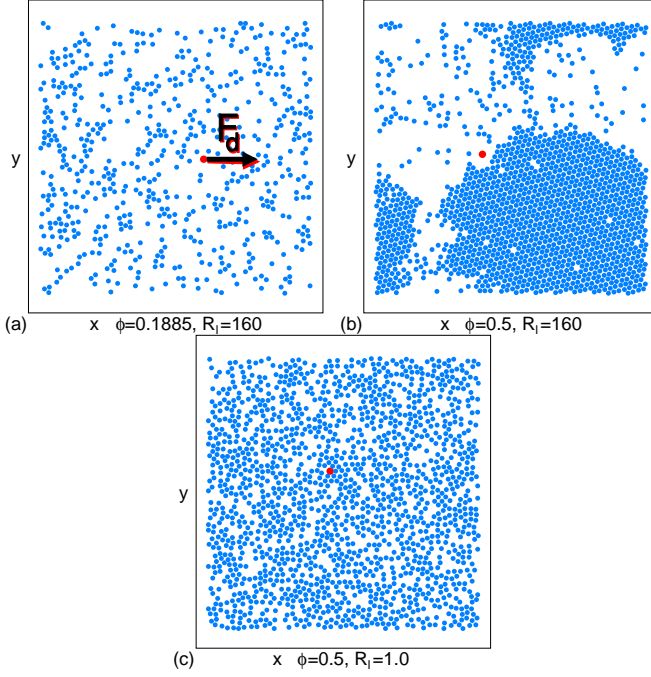


FIG. 1: Particle locations for an active matter system with an externally driven probe particle (red). (a) Uniform liquid state at $\phi = 0.1885$ and $R_l = 160$. Arrow: direction of the probe driving force F_d . (b) Phase-separated cluster state at $\phi = 0.5$ and $R_l = 160$ consisting of a high density phase with local crystal ordering coexisting with a low density liquid phase. (c) The uniform liquid phase at $\phi = 0.5$ and $R_l = 1.0$

reduced mobility. Here the probe velocity often drops to zero and the probe moves only in intermittent bursts or avalanches with size distributions that can be fit to a power law. These results suggest that, at least in the high density regime, the addition of activity can induce critical behavior similar to the type associated with jamming in granular systems^{16–18,43,44}.

II. SIMULATION

We consider a two-dimensional system of size $L \times L$ with periodic boundary conditions containing N run-and-tumble monodisperse disks of radius r_d that interact via a repulsive harmonic potential. The density of particles is given by $\phi = N\pi r_d^2/L^2$, where we take $L = 50$ and $r_d = 0.5$ in dimensionless simulation units. In the absence of activity, a hexagonal solid forms when $\phi > 0.9$. The dynamics of a single particle i is obtained by integrating the overdamped equation of motion

$$\eta \frac{d\mathbf{R}_i}{dt} = \mathbf{F}_i^m + \mathbf{F}_i^s. \quad (1)$$

Here $\eta = 1.0$ is the damping constant and \mathbf{F}_i^m is the motor force, which drives the particle in a fixed randomly chosen direction under a force of magnitude $F_m = 0.5$

during a run time τ_r . A new running direction is randomly selected after each run time. The run length $R_l \equiv F_m \tau_r$ is the distance the particle would move in the absence of other particles. The steric interactions are given by $\mathbf{F}_i^s = \sum_{j \neq i}^N (k/r_d)(R_{\text{eff}} - |\mathbf{r}_{ij}|)\Theta(R_{\text{eff}} - |\mathbf{r}_{ij}|)\hat{\mathbf{r}}_{ij}$, where $\mathbf{r}_{ij} = \mathbf{R}_i - \mathbf{R}_j$, $\hat{\mathbf{r}}_{ij} = \mathbf{r}_{ij}/|\mathbf{r}_{ij}|$, $k = 20$, $R_{\text{eff}} = 2r_d$, and $\mathbf{R}_{i(j)}$ is the location of particle $i(j)$. We add a single non-active probe particle with $F^m = 0$ to the system with the same radius and steric interactions as the active particles and apply a constant force $\mathbf{F}_d = F_d \hat{\mathbf{x}}$ with $F_d = 0.5$ to only the probe particle, as shown in Fig. 1(a). Since we are using overdamped dynamics, we employ a forward Euler method to advance the equations of motion with an integration step of $\delta t = 0.001$ dimensionless simulation time units. We have considered other values of F_m and find that, outside the limits $F_d \gg F_m$ or $F_d \ll F_m$, the general features of our results are robust against the exact choice of F_d/F_m . We initialize the system by placing the particles in non-overlapping randomly chosen positions. In active matter particle systems, it is known that in the regime where the system forms clumps or becomes phase separated, there can be long transient times before the sample reaches a steady state^{37,46}. In all cases, prior to taking measurements we wait a sufficient time for the system to settle into a steady state, as determined by measuring when the probe particle velocity and the fraction of sixfold coordinated particles $P_6 = \sum_i^N \delta(z_i - 6)$, where z_i is the coordination number of an individual particle as obtained from a Voronoi construction, settle onto a steady state value. The length of the transient time depends on the density and run length, and ranges from 10^3 simulation time steps in the liquid phase up to 10^6 or more simulation time steps in the dense phase. We note that we consider systems containing up to $N = 11000$ particles, which limits the size of the transient times compared to the considerably larger number of particles employed in^{37,46}.

To characterize the system we measure the time series of the probe velocity fluctuations $V_x(t) = (d\mathbf{R}_p/dt) \cdot \hat{\mathbf{x}}$, where \mathbf{R}_p is the probe position. In the absence of any other particles, $F_d/\langle V_x \rangle = 1.0$. In previous simulations of the same run-and-tumble system performed with no probe particle, a transition from a liquid state to a cluster state occurred for fixed ϕ and increasing R_l , or for fixed R_l and increasing ϕ ⁴⁰. Very similar results have been obtained for active Brownian particles, where at a fixed density a transition to a cluster state occurs for increasing persistence length^{36,37}. It has been shown that run-and-tumble dynamics and active Brownian motion produce equivalent results when the mobility of the particles is density dependent⁴⁵, which occurs when particle-particle interactions are present, so we expect our results to be general to either type of system.

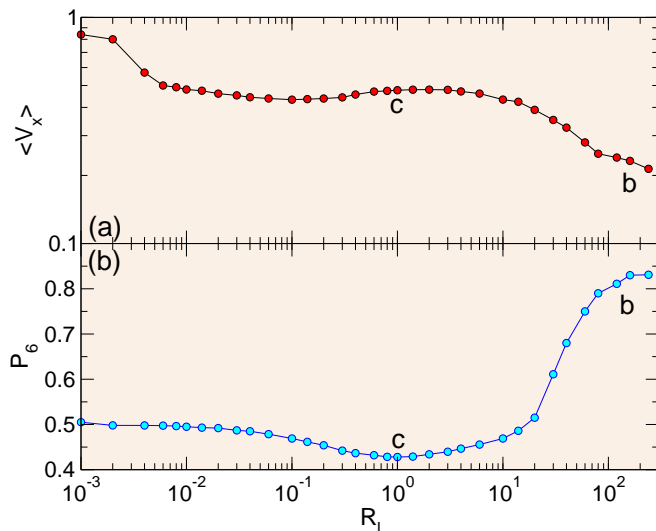


FIG. 2: (a) Mobility $\langle V_x \rangle$ of the probe particle vs run length R_l for the system from Fig. 1(b,c) with $\phi = 0.5$. (b) Corresponding fraction of six-fold coordinated particles P_6 vs R_l . The $R_l = 160$ point illustrated in Fig. 1(b), where the system is phase separated and the probe particle mobility is low, is marked **b**, while the $R_l = 1$ point illustrated in Fig. 1(c), where the system is in a liquid state and the mobility is higher, is marked **c**.

III. PROBE MOBILITY VS RUN LENGTHS AND ϕ

We first consider the mobility of the probe particle by fixing F_d and conducting a series of simulations for varied particle density ϕ and varied run length R_l . As a point of reference, note that nonactive disks with $R_l = 0$ form a triangular solid at a density of $\phi = 0.9$. In Fig. 1(a) we show snapshots of the active and drive particle positions in a uniform liquid state at $\phi = 0.1885$ and $R_l = 160$. When the run length is held constant but the density is increased, the system no longer remains a uniform liquid but instead forms a phase separated or cluster state, as shown in Fig. 1(b) at $\phi = 0.5$ and $R_l = 160$. Within an individual cluster, the local density ϕ_{loc} is just below $\phi_{\text{loc}} = 0.9$ and there is considerable hexagonal ordering of the particles. The clusters are not static but gradually change over time. For $\phi = 0.5$, the cluster state appears when $R_l > 30$. Figure 1(c) illustrates a sample with $\phi = 0.5$ and $R_l = 1.0$. Here the run length is small enough that the clusters are lost and a uniform liquid reappears.

In Fig. 2(a) we plot the mobility $\langle V_x \rangle$ of the probe particle as a function of R_l for the system with $\phi = 0.5$ illustrated in Fig. 1(b,c). In order to correlate the mobility with different dynamical structures in the active media, in Fig. 2(b) we plot the corresponding fraction of sixfold-coordinated particles P_6 versus R_l . In the disordered liquid state for low R_l , P_6 is low, while in the cluster state $P_6 > 0.8$ since, within the clusters, most par-

ticles have six neighbors. The mobility initially decreases with increasing R_l in the range $0.001 < R_l < 0.01$, passing through a local minimum near $R_l = 0.1$. For $0.3 < R_l < 8$ there is small increase in $\langle V_x \rangle$, while for $R_l > 8$ the mobility rapidly decreases with increasing R_l . In Fig. 2(b), there is a local minimum in P_6 near $R_l = 1.0$ which coincides with the local maximum in the mobility shown in Fig. 2(a). For $R_l > 8.0$, P_6 begins to grow rapidly with increasing R_l , indicating the onset of cluster formation. The rise in P_6 corresponds with a decrease in the mobility in Fig. 2(a). At very low R_l the system acts like a zero temperature non-active system through which the probe particle can easily move. As R_l increases for fixed ϕ , the probe particle encounters active particles more frequently, decreasing its mobility. The system becomes more disordered as R_l increases, reaching a maximally disordered state at $R_l = 1$. The liquid nature of the disordered state permits the probe particle to move more easily through the sample, giving a small increase in the mobility.

Once clusters begin to form for $R_l > 8$, the probe particle often becomes trapped within a cluster. During this trapped period, the motion of the particle in the driving direction drops nearly to zero, so that a probe particle caught in a cluster is effectively in a locally jammed state. Here, the term jamming refers to the impedance of motion due to steric interparticle interactions. Since the clusters are dynamical in nature, the driven particle eventually escapes from the cluster and promptly moves much more rapidly as it passes through the low density liquid phase that surrounds the clusters. As R_l increases, individual clusters become longer-lived, so the probe spends larger amounts of time trapped inside clusters in a low mobility state, resulting in a net decrease of the average mobility with increasing R_l .

The nonmonotonic behavior of the mobility with R_l also depends on ϕ . In Fig. 3(a) we plot $\langle V_x \rangle$ versus R_l for a system with $\phi = 0.801$. For $0.001 < R_l < 0.01$, there is a decrease in the mobility with increasing R_l which becomes more pronounced for $R_l > 0.01$ before $\langle V_x \rangle$ reaches a local minimum near $R_l = 0.005$. For $R_l > 1.0$ the mobility sharply increases with increasing R_l to a local maximum near $R_l = 2.0$. The total drop and recovery of $\langle V_x \rangle$ between $R_l = 0.01$ and $R_l = 1$ covers more than an order of magnitude. In Fig. 3(b) we plot the corresponding P_6 versus R_l , where for $0.001 \leq R_l < 0.01$, P_6 increases with increasing R_l , indicating that the activity is producing additional order in the system. For $0.01 < R_l < 0.02$, there is a local maximum in P_6 with $P_6 = 0.99$, indicating almost perfect triangular ordering of the system. This same interval of R_l also corresponds to the low mobility region in Fig. 3(a), as highlighted by the vertical dashed lines. The peak in the mobility centered near $R_l = 2.0$ is matched by a local minimum in P_6 in Fig. 3(b), indicating that the activity has now disordered the system. There is no sharp signature in P_6 at the onset of the phase separated state, but P_6 increases with increasing R_l in this regime as the mobility drops.

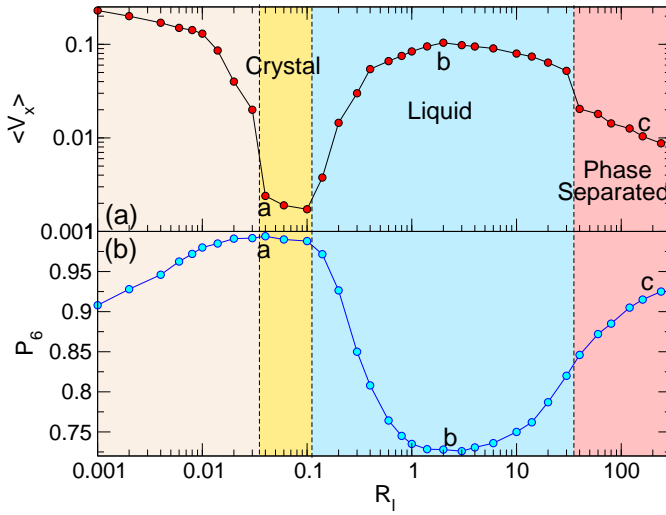


FIG. 3: (a) $\langle V_x \rangle$ vs R_l for a system with $\phi = 0.801$. (b) The corresponding P_6 vs R_l . Point **a**, in the crystalline phase where the mobility is low, is illustrated in Fig. 4(a). Point **b**, in the liquid phase where the mobility is high, is illustrated in Fig. 4(b). Point **c**, in the clump or phase separated phase where the mobility decreases again, is illustrated in Fig. 4(c).

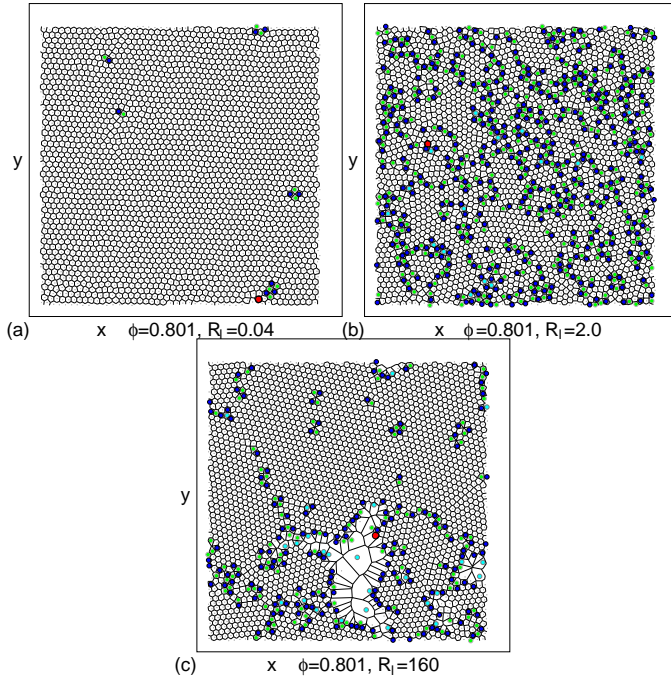


FIG. 4: Voronoi construction images for the system in Fig. 3 with $\phi = 0.801$. Particle coordination numbers: $z_i = 5$ (dark blue), $z_i = 6$ (white), $z_i = 7$ (green), $z_i \geq 8$ (light blue). The driven particle is marked with a red dot. (a) At $R_l = 0.04$, labeled **a** in Fig. 3, the system forms a crystallized state. (b) At $R_l = 2.0$, labeled **b** in Fig. 3, the system forms a disordered uniform liquid state. (c) At $R_l = 160$, labeled **c** in Fig. 3, the system forms a phase separated state with high density clusters and a low density gas of particles.

Figure 4(a) shows the Voronoi construction obtained from the particle positions for the system in Fig. 3 at $\phi = 0.801$ and $R_l = 0.04$. Although $\phi = 0.801$ is well below the non-active crystallization density of $\phi = 0.9$, we find a uniform activity-stabilized triangular lattice interspersed with a small number of defects. The fact that the probe particle mobility drops nearly to zero in this regime indicates that this phase behaves like a solid. This crystalline state is distinct from the cluster phase in that it is completely uniform and appears at much lower values of R_l . The crystallization occurs only when ϕ is relatively high, so that each particle can be regarded, on average, as filling ϕ percent of a hexagon of side l_b centered on the particle: $l_b = \sqrt{2\pi r_d^2 / (3\sqrt{3}\phi)}$. Then the average surface-to-surface spacing between neighboring particles is $d_s = l_b - r_d$. For $\phi = 0.801$, $d_s = 0.11$. Since all of the particles are actively moving, a collision occurs every time the particles traverse an average distance of $r_s = d_s/2 = 0.055$. When $R_l \sim r_s$, there is a matching effect in which each particle is struck, on average, nearly uniformly around its circumference by neighboring particles, resulting in the formation of the crystalline state. If ϕ decreases, r_s becomes large enough that multiple collisions between neighboring particles can occur as a particle moves the corresponding distance R_l , so the crystalline ordering is lost. The crystallization is accompanied by a maximum in P_6 in Fig. 3(b). When $R_l \ll r_s$, the system is in an unjammed disordered state and the probe particle can move easily through the sample.

Although the activity can induce a crystallization when $R_l \approx r_s$, if R_l increases too much the forces exerted on a given particle by its neighbors are no longer symmetric; instead, an unbalanced excess force arises whenever a long-lived contact with another particle forms for two particles swimming in opposite directions toward each other. Thus the crystalline order is lost when R_l is too large, as illustrated in Fig. 4(b) for $R_l = 2.0$. The disordering of the system appears as a drop in P_6 in Fig. 3(b), and Fig. 4(b) shows that the sample enters a uniform active liquid state containing numerous dislocations. Since the system is now a liquid instead of a solid, the probe particle can pass through the sample much more easily and the mobility in Fig. 3(a) increases. As R_l is further increased, the system enters the cluster phase where large regions of the sample have sixfold ordering, as illustrated in Fig. 4(c) for $\phi = 0.801$ and $R_l = 160$. At the corresponding density in Fig. 3, P_6 is large again and the mobility is low. The decrease in average mobility occurs since the velocity of the probe particle drops nearly to zero whenever it traverses a dense portion of the sample.

In Fig. 5(a) we plot $\langle V_x \rangle$ versus R_l for ϕ ranging from $\phi = 0.1885$ to $\phi = 0.8482$, while in Fig. 5(b) we show corresponding P_6 versus R_l . There is a pronounced minimum in $\langle V_x \rangle$ for the $\phi = 0.801$ and $\phi = 0.8482$ curves due to the occurrence of activity-induced crystallization as described above. A small residue of this effect remains at $\phi = 0.754$. For $1 < R_l < 30$, the system is in a disordered liquid state at all the values of ϕ , while

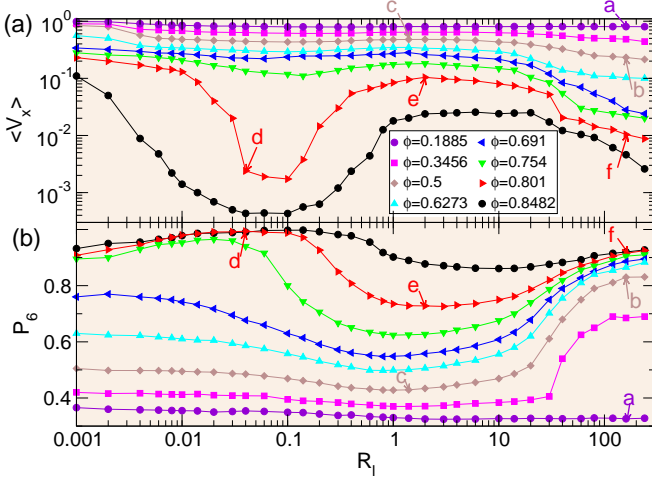


FIG. 5: (a) Mobility $\langle V_x \rangle$ of the probe vs run length R_l for $\phi = 0.1885, 0.3456, 0.5, 0.6273, 0.691, 0.754, 0.801$, and 0.8482 , from top to bottom. (b) Corresponding P_6 vs R_l for $\phi = 0.1885, 0.3456, 0.5, 0.6273, 0.691, 0.754, 0.801$, and 0.8482 , from bottom to top.

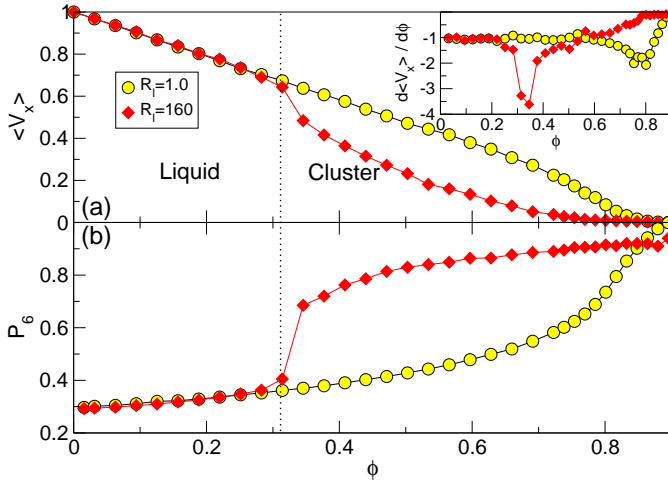


FIG. 6: (a) Mobility $\langle V_x \rangle$ vs ϕ for $R_l = 1.0$ (circles) and $R_l = 160$ (diamonds). Inset: corresponding $d\langle V_x \rangle/d\phi$. (b) P_6 vs ϕ . Dashed line indicates the correspondence between the clustering onset and the mobility drop.

for $R_l > 30$, the increase in P_6 indicates that the system is entering the clump phase in which the mobility drops. For $\phi = 0.1885$, the system remains in the liquid phase over the entire range of R_l and shows little change in $\langle V_x \rangle$ or P_6 . These results indicate that the activity induced crystallization at low R_l only occurs when ϕ is sufficiently large, whereas the cluster phase at large R_l appears over a wide range of ϕ .

To further characterize the change in the mobility with the onset of clustering and ordering, in Fig. 6 we plot $\langle V_x \rangle$ and P_6 versus ϕ for samples with $R_l = 160$ and $R_l = 1.0$. For $0 < \phi < 0.3$, $\langle V_x \rangle$ is independent of R_l and decreases

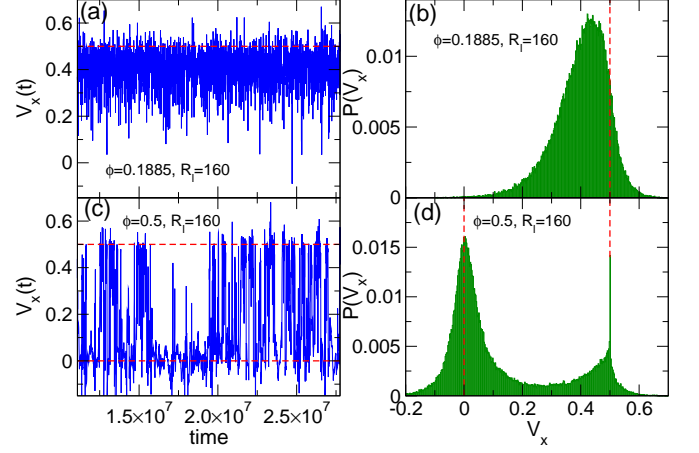


FIG. 7: (a) Portion of a probe velocity time series $V_x(t)$ in the uniform liquid state at $\phi = 0.1885$ and $R_l = 160$. The dashed line indicates the free probe velocity $V_0 = F_d = 0.5$. (b) The probability distribution of the velocity fluctuations $P(V_x)$ from (a). (c) Portion of $V_x(t)$ in the phase separated state at $\phi = 0.5$ and $R_l = 160$ where two-level fluctuations occur. (d) $P(V_x)$ from (c) showing peaks at $V_x = 0.0$ and $V_x = V_0 = 0.5$.

linearly with increasing ϕ . For $\phi > 0.3$, the $R_l = 160$ system undergoes a transition to the cluster state, producing a sharp increase in P_6 and a simultaneous mobility drop. As ϕ increases, $\langle V_x \rangle$ in the $R_l = 1.0$ system decreases linearly, while in the $R_l = 160$ system $\langle V_x \rangle$ drops rapidly in the cluster phase until becoming nearly zero for $\phi > 0.75$. In the inset of Fig. 6(a), the plot of $d\langle V_x \rangle/d\phi$ versus ϕ shows the much earlier mobility drop of the $R_l = 160$ system compared to the $R_l = 1.0$ system, where the drop does not occur until $\phi \approx 0.8$. Near $\phi = 0.6$, Fig. 6(a) shows that $\langle V_x \rangle$ in the $R_l = 160$ system is more than ten times smaller than in the $R_l = 1$ system. Close to the hard sphere crystallization density of $\phi = 0.9$, the two systems have nearly equal mobilities.

IV. VELOCITY FLUCTUATION DISTRIBUTIONS

We next examine the velocity fluctuation distributions of the probe particle. In Fig. 7(a) we plot a representative portion of the probe velocity time series $V_x(t)$ in the liquid phase from Fig. 1(a) at $\phi = 0.1885$ and $R_l = 160$. The dashed line in Fig. 7(a) indicates the velocity $V_0 = F_d = 0.5$ at which the probe particle would move in the absence of the active bath particles. Figure 7(b) shows that the corresponding probability distribution function $P(V_x)$ has a skewed Gaussian shape with a maximum near $V_x = 0.425$. We find similar $P(V_x)$ distributions in other uniform liquid states. For lower values of ϕ , a peak in $P(V_x)$ at $V = V_0$ begins to emerge when the probe particle moves large distances before encountering another particle. Figure 7(c) shows $V_x(t)$ for

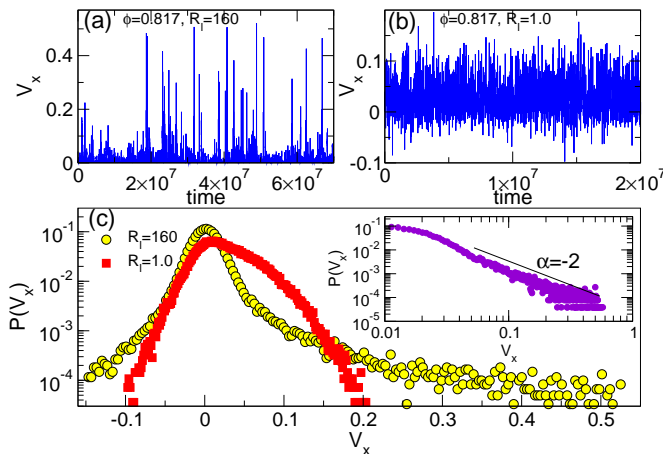


FIG. 8: (a) Portion of $V_x(t)$ in the active jamming phase at $\phi = 0.817$ and $R_l = 160$ showing that the probe particle moves in discrete jumps or avalanches. (b) $V_x(t)$ in the uniform liquid state at $\phi = 0.817$ and $R_l = 1.0$ where the probe moves continuously. (c) Log-linear plot of $P(V_x)$ from the time series at $\phi = 0.817$ with $R_l = 160$ (circles) and $R_l = 1.0$ (squares). Inset: log-log plot of $P(V_x)$ for the positive V_x values at $R_l = 160$. Solid line: a power law fit with exponent $\alpha = -2.0$.

$\phi = 0.5$ and $R_l = 160$ when the sample is in the cluster phase illustrated in Fig. 1(b). Here the noise fluctuations are of two-level or telegraph type, and V_x jumps between the values $V_x = 0.0$ and $V_x = V_0 = 0.5$, highlighted by the dashed lines. The resulting $P(V_x)$ contains two clear peaks, as shown in Fig. 7(d). The two-level behavior arises because the probe velocity is nearly zero when the probe becomes trapped in a cluster, and nearly V_0 when the probe moves through the low density gas surrounding the clusters where it undergoes very few collisions. The peak at $V_x = 0.5$ for $\phi = 0.5$ in Fig. 7(d) is quite sharp, whereas the peak in $P(V_x)$ at $\phi = 0.1885$ in Fig. 7(b) is centered at $V_x = 0.425$ even though the system is in a low density liquid phase. The difference in peak sharpness arises because the liquid density at $\phi = 0.1885$, although low, is considerably higher than the density in the gas state surrounding the clusters that form at $\phi = 0.5$, and the resulting larger number of probe-bath particle encounters in the liquid state broaden the peak relative to its width in the gas state. We observe similar telegraph noise distributions in the other phase separated regimes for $R_l = 160$ over the range $0.377 < \phi < 0.75$, and find that the weight of the distribution shifts from the $V_x = 0.5$ peak to the $V_x = 0.0$ peak as ϕ increases. The telegraph noise signal can be viewed as a linear combination of the velocity fluctuation distributions from the low density phase, which has a skewed Gaussian shape with a peak near the driving value of $F_d = 0.5$, and the high density phase, which has one peak centered at zero and a second peak centered at 0.5, similar to the shape shown in Fig. 7(d).

For $\phi > 0.75$ and $R_l = 160$, the probe is mostly sta-

tionary and only moves in short bursts or avalanches with a broad distribution of jump sizes. This is illustrated by the plot of $V_x(t)$ in Fig. 8(a) for $\phi = 0.817$ and $R_l = 160$. If ϕ is held fixed and R_l is reduced to $R_l = 1.0$, the system forms a disordered liquid state and the probe motion is no longer intermittent, as shown in the plot of $V_x(t)$ in Fig. 8(b). Figure 8(c) illustrates the corresponding $P(V_x)$ curves on a log-linear scale for $R_l = 1.0$ and $R_l = 160$. For $R_l = 160$, $P(V_x)$ has a pronounced peak near $V_x = 0.0$ and a broad tail for $V_x > 0.1$, while for $R_l = 1.0$, $P(V_x)$ falls off more rapidly for $V_x > 0.1$ and the maximum is centered slightly higher than $V_x = 0.0$. The inset of Fig. 8(c) shows a log-log plot of $P(V_x)$ for positive values of V_x at $R_l = 160$. The solid line is a power law fit to the form $P(V_x) \propto V_x^{-2}$. Similar fits can be made for $\phi > 0.75$ and $R_l = 160$.

We characterize the $\phi > 0.75$ and $R_l > 30$ regime as actively jammed, since this is where the probe particle velocity is power-law distributed. For non-active matter systems very near the jamming transition, a driven probe particle also moves in an intermittent fashion and undergoes avalanches with a size distribution that can be fit to a power law^{17,18}. The active matter avalanche behavior suggests that the active system shares characteristics with a jammed phase, but that these characteristics arise at densities well below the non-active jamming density. Jamming behavior of non-active disks has been widely studied for bidisperse, rather than monodisperse, disk sizes, which produce a disordered structure at high densities. Jamming has been used as a general concept for describing amorphous solids. In the phase-separated active matter system, the dense regions of the sample are polycrystalline rather than amorphous; however, the polycrystalline structures are not static but dynamically change, so that the system can be regarded as dynamically amorphous. Images of the states that form at high ϕ and large R_l show the formation of various grain boundary structures, implying that a probe motion avalanche might occur whenever a grain boundary passes over the probe particle. There are, however, also other types of defects and small voids present that can also affect the probe particle motion. In addition, the probe particle can itself nucleate local topological defects and voids, which then interact with the motion of the probe particle. It is beyond the scope of this work to definitively determine whether the dense active phase is truly in a critical state; however, the observed power-law exponent of $\alpha = -2.0$ is consistent with the class of time-directed avalanche systems⁴⁸. Future directions include studying polydisperse active particle assemblies, active rods, or active dumbbells.

V. CONCLUSION

In conclusion, we have examined the mobility and velocity fluctuations of an externally driven probe particle moving through a bath of active matter disks for varied

activity and particle density. As a function of increasing run length, we show that there is a pronounced drop in the probe particle mobility at the transition from a uniform liquid state to a cluster or phase separated state. The mobility reduction in the cluster state arises due to the temporary trapping of the probe particle by dense clusters. When the probe particle escapes a cluster, it moves with a much higher, nearly free mobility until it encounters another cluster. The time series of the velocity in the uniform liquid regime exhibits a skewed Gaussian shape, while in the phase separated regime we observe two-level velocity fluctuations as the particle jumps between dense low mobility regions of the sample and gas-like high mobility regions of the sample. As the density of active particles increases, we find strongly nonmonotonic behavior of the probe particle mobility as a function of run length. For finite but small run lengths, the mobility initially drops by nearly two orders of magnitude when the system enters an activity-induced crystallization regime. As the run length increases, the crystalline state becomes unstable, the system disorders, and the mobility can increase by a few orders of magnitude.

At the largest run lengths the system enters the phase separated regime and the mobility of the probe particle decreases again. We also find that in samples with high densities and large run lengths, the probe particle moves in an intermittent fashion via discrete jumps or avalanches, and that the probe velocity is power-law distributed. The avalanche velocity distributions suggest that the dense active system may exhibit a critical behavior similar to that found for a probe particle moving through a non-active disordered 2D assembly just below the jamming transition. Our results should be general to both run-and-tumble active systems as well as active Brownian particles.

Acknowledgments

This work was carried out under the auspices of the NNSA of the U.S. DoE at LANL under Contract No. DE-AC52-06NA25396.

-
- ¹ T.M. Squires and J.F. Brady, *Phys. Fluids* **17**, 073101 (2005).
 - ² A. Meyer, A. Marshall, B.G. Bush, and E.M. Furst, *J. Rheol.* **50**, 77 (2006).
 - ³ L.G. Wilson and W.C.K. Poon, *Phys. Chem. Chem. Phys.* **13**, 10617 (2011).
 - ⁴ A.M. Puertas and Th. Voigtmann, *J. Phys.: Condens. Matter* **26**, 243101 (2014).
 - ⁵ P. Habdas, D. Schaar, A.C. Levitt, and E.R. Weeks, *Europhys. Lett.* **67**, 477 (2004).
 - ⁶ M.B. Hastings, C.J. Olson Reichhardt, and C. Reichhardt, *Phys. Rev. Lett.* **90**, 098302 (2003).
 - ⁷ I. Gazuz, A.M. Puertas, Th. Voigtmann, and M. Fuchs, *Phys. Rev. Lett.* **102**, 248302 (2009).
 - ⁸ D. Winter, J. Horbach, P. Virnau, and K. Binder, *Phys. Rev. Lett.* **108**, 028303 (2012).
 - ⁹ C.F.E. Schroer and A. Heuer, *Phys. Rev. Lett.* **110**, 067801 (2013).
 - ¹⁰ P. Illien, O. Bénichou, G. Oshanin, and R. Voituriez, *Phys. Rev. Lett.* **113**, 030603 (2014).
 - ¹¹ C. Reichhardt and C.J. Olson Reichhardt, *Phys. Rev. Lett.* **96**, 028301 (2006).
 - ¹² H.H. Wensink and H. Löwen, *Phys. Rev. Lett.* **97**, 038303 (2006).
 - ¹³ O. Bénichou, C. Mejía-Monasterio, and G. Oshanin, *Phys. Rev. E* **87**, 020103 (2013).
 - ¹⁴ C. Reichhardt and C.J. Olson Reichhardt, *Phys. Rev. Lett.* **92**, 108301 (2004).
 - ¹⁵ R.P.A. Dullens and C. Bechinger, *Phys. Rev. Lett.* **107**, 138301 (2011).
 - ¹⁶ J.A. Drocco, M.B. Hastings, C.J. Olson Reichhardt, and C. Reichhardt, *Phys. Rev. Lett.* **95**, 088001 (2005).
 - ¹⁷ R. Candelier and O. Dauchot, *Phys. Rev. Lett.* **103**, 128001 (2009).
 - ¹⁸ C.J. Olson Reichhardt and C. Reichhardt, *Phys. Rev. E* **82**, 051306 (2010).
 - ¹⁹ E. Kolb, P. Cixous, N. Gaudouen, and T. Darnige, *Phys. Rev. E* **87**, 032207 (2013).
 - ²⁰ Y. Takehara and K. Okumura, *Phys. Rev. Lett.* **112**, 148001 (2014).
 - ²¹ S. Ramaswamy, *Annu. Rev. Condens. Matter Phys.* **1**, 323 (2010).
 - ²² M.C. Marchetti, J.F. Joanny, S. Ramaswamy, T.B. Liverpool, J. Prost, M. Rao, and R.A. Simha, *Rev. Mod. Phys.* **85**, 1143 (2013).
 - ²³ H.C. Berg, *Random Walks in Biology* (Princeton University Press, Princeton, 1983).
 - ²⁴ P. Galajda, J. Keymer, P. Chaikin, and R. Austin, *J. Bacteriol.* **189**, 8704 (2007).
 - ²⁵ M.B. Wan, C.J. Olson Reichhardt, Z. Nussinov, and C. Reichhardt, *Phys. Rev. Lett.* **101**, 018102 (2008).
 - ²⁶ L. Angelani, R. DiLeonardo, and G. Ruocco, *Phys. Rev. Lett.* **102**, 048104 (2009).
 - ²⁷ W.F. Paxton *et al.*, *J. Am. Chem. Soc.* **126**, 13424 (2004).
 - ²⁸ J.R. Howse, R.A.L. Jones, A.J. Ryan, T. Gough, R. Vafabakhsh, and R. Golestanian, *Phys. Rev. Lett.* **99**, 048102 (2007).
 - ²⁹ R. Golestanian, *Phys. Rev. Lett.* **102**, 188305 (2009).
 - ³⁰ H.R. Jiang, N. Yoshinaga, and M. Sano, *Phys. Rev. Lett.* **105**, 268302 (2010).
 - ³¹ G. Volpe, I. Buttinoni, D. Vogt, H.-J. Kümmerer, and C. Bechinger, *Soft Matter* **7**, 8810 (2011).
 - ³² J. Palacci, S. Sacanna, A.P. Steinberg, D.J. Pine, and P.M. Chaikin, *Science* **339**, 936 (2013).
 - ³³ I. Buttinoni, J. Bialké, F. Kümmel, H. Löwen, C. Bechinger, and T. Speck, *Phys. Rev. Lett.* **110**, 238301 (2013).
 - ³⁴ A.G. Thompson, J. Tailleur, M.E. Cates, and R.A. Blythe, *J. Stat. Mech.: Theor. Exp.* **2011**, P02029 (2011).
 - ³⁵ J. Bialké, T. Speck, and H. Löwen, *Phys. Rev. Lett.* **108**,

- 168301 (2012).
- ³⁶ Y. Fily and M.C. Marchetti, Phys. Rev. Lett. **108**, 235702 (2012).
- ³⁷ G.S. Redner, M.F. Hagan, and A. Baskaran, Phys. Rev. Lett. **110**, 055701 (2013).
- ³⁸ B.M. Mognetti, A. Saric, S. Angioletti-Uberti, A. Cacciuto, C. Valeriani, and D. Frenkel, Phys. Rev. Lett. **111**, 245702 (2013).
- ³⁹ D. Levis and L. Berthier, Phys. Rev. E **89**, 062301 (2014).
- ⁴⁰ C. Reichhardt and C.J. Olson Reichhardt, Phys. Rev. E **90**, 012701 (2014).
- ⁴¹ G. Foffano, J.S. Lintuvuori, K. Stratford, M.E. Cates, and D. Marenduzzo, Phys. Rev. Lett. **109**, 028103 (2012).
- ⁴² B. Wang, J. Kuo, and S. Granick, Phys. Rev. Lett. **111**, 208102 (2013).
- ⁴³ A.J. Liu and S.R. Nagel, Nature (London) **396**, 21 (1998).
- ⁴⁴ C.S. O'Hern, L.E. Silbert, A.J. Liu, and S.R. Nagel, Phys. Rev. E **68**, 011306 (2003).
- ⁴⁵ M.E. Cates and J. Tailleur, EPL **101**, 20010 (2013).
- ⁴⁶ J. Stenhammer, D. Marenduzzo, R. J. Allen, and M.E. Cates Soft Matter **10**, 14898 (2014).
- ⁴⁷ D. Helbing, I.J. Farkas, and T. Vicsek, Phys. Rev. Lett. **84**, 1240 (2000).
- ⁴⁸ S. Maslov, Phys. Rev. Lett. **74**, 562 (1995).